

~~CONFIDENTIAL~~

Copy 401  
RM L58A21

NACA RM L58A21



# RESEARCH MEMORANDUM

WIND-TUNNEL INVESTIGATION AT A MACH NUMBER OF 2.01 OF  
THE AERODYNAMIC CHARACTERISTICS IN COMBINED ANGLES  
OF ATTACK AND SIDESLIP OF SEVERAL HYPERSONIC  
MISSILE CONFIGURATIONS WITH VARIOUS

CANARD CONTROLS

By Ross B. Robinson

Langley Aeronautical Laboratory  
Langley Field, Va.

N65-24057

(ACCESSION NUMBER)

35  
(PAGES)

(THRU)

(CODE)

01  
(CATEGORY)

(NASA CR OR TMX OR AD NUMBER)

DECLASSIFIED: Effective 2-5-65  
Authority: F.G. Drobka (ATSS-A,  
memo dated 3-25-65: AFDDO-5197



## NATIONAL ADVISORY COMMITTEE FOR AERONAUTICS

WASHINGTON

March 10, 1958

Hard copy (HC) \$2.00

Microfiche (MF) .50





---

RESEARCH MEMORANDUM

---

WIND-TUNNEL INVESTIGATION AT A MACH NUMBER OF 2.01 OF  
THE AERODYNAMIC CHARACTERISTICS IN COMBINED ANGLES  
OF ATTACK AND SIDESLIP OF SEVERAL HYPERSONIC  
MISSILE CONFIGURATIONS WITH VARIOUS  
CANARD CONTROLS

By Ross B. Robinson

SUMMARY

24057

An investigation of the aerodynamic characteristics of several hypersonic missile configurations with various canard controls for an angle-of-attack range from  $0^\circ$  to about  $28^\circ$  at sideslip angles of about  $0^\circ$  and  $4^\circ$  at a Mach number of 2.01 has been made in the Langley 4- by 4-foot supersonic pressure tunnel. The configurations tested were a body alone which had a ratio of length to diameter of 10, the body with a  $10^\circ$  flare, the body with cruciform fins of  $5^\circ$  or  $15^\circ$  apex angle, and a flare-stabilized rocket model with a modified Von Kármán nose. Various canard surfaces for pitch control only were tested on the body with the  $10^\circ$  flare and on the body with both sets of fins.

The results indicated that the addition of a flared afterbody or cruciform fins produced configurations which were longitudinally and directionally stable. The body with  $5^\circ$  fins should be capable of producing higher normal accelerations than the flared body. All of the canard surfaces were effective longitudinal controls which produced net positive increments of normal force and pitching moments which progressively decreased with increasing angle of attack.

INTRODUCTION

One of the requirements for ground-to-air and air-to-air missiles is the attainment of large flight-path changes and high normal accelerations that are necessary for target acquisition. In addition, when used

A large black redaction mark is placed at the bottom of the page, covering several lines of text.

against targets that may be operating at supersonic speeds, the missile must have a large speed advantage and may be required to operate at hypersonic speeds. At these speeds, not only are the aerodynamic and control problems complicated, but problems of aerodynamic heating will also be encountered.


Among the configurations that are being considered for hypersonic missiles are those having highly swept wings of low aspect ratio since some investigations (for example, refs. 1 to 3) indicate that configurations of this type have some distinct advantages. These advantages include high lift effectiveness, little drag penalty with shapes that appear to be beneficial for decreasing aerodynamic heating, small center-of-pressure shifts, and small induced rolling moments. In addition, the results of reference 1 indicate that wingless missiles with flared afterbodies may be satisfactory from a stability standpoint, although the lift capabilities are low and the drag penalty is high.

In order to obtain more information on the stability and control characteristics of configurations that offer promise as hypersonic missiles, an investigation of a family of missile models has been undertaken by the National Advisory Committee for Aeronautics. The initial phase of the investigation has included tests in the Langley 4- by 4-foot supersonic pressure tunnel and the Langley Unitary Plan wind tunnel for the Mach number range from 2.01 to 4.65. The family of models investigated included a body alone having a length-to-diameter ratio of 10, the body with a  $10^\circ$  flared afterbody, and the body with two different sets of low-aspect-ratio cruciform fins. The fins had a ratio of span to body diameter of 2.067 and had apex angles of  $5^\circ$  and  $15^\circ$ . An additional model was included to simulate a Langley Pilotless Aircraft Research Division free-flight hypersonic test vehicle. (See ref. 4.) This model was wingless and had a ratio of body length to diameter of 11.70, a  $10^\circ$  flared afterbody, and a modified Van Kármán nose.

This paper presents the results of the investigation of these models at a Mach number of 2.01 in the Langley 4- by 4-foot supersonic pressure tunnel. In addition to the family of models previously described, this investigation included control studies with three different canard surfaces for pitch control only on the body with the flare and the body with both sets of wings. Six-component force and moment data were obtained for combined angles of attack and sideslip up to about  $28^\circ$  and for control deflection angles up to about  $20^\circ$ .

#### SYMBOLS

The data are presented as coefficients of forces and moments with the center of moments at the 50-percent body station. All of the data



are referred to the body axis system (fig. 1).

$C_N$	normal-force coefficient, $F_N/q_S$
$C_A$	axial-force coefficient, $F_A/q_S$
$C_m$	pitching-moment coefficient, $M_Y/q_S d$
$C_l$	rolling-moment coefficient, $M_X/q_S d$
$C_n$	yawing-moment coefficient, $M_Z/q_S d$
$C_Y$	side-force coefficient, $F_Y/q_S$
$F_N$	normal force
$F_A$	axial force
$F_Y$	side force
$M_X$	rolling moment
$M_Y$	pitching moment
$M_Z$	yawing moment
$d$	diameter of cylindrical section of body
$S$	cross-sectional area of cylindrical section of body
$x$	distance rearward from nose
$R$	radius
$q$	free-stream dynamic pressure
$\alpha$	angle of attack of body center line, deg
$\beta$	angle of sideslip of body center line, deg
$\delta_c$	deflection angle of canard with respect to body center line, positive when trailing edge down, deg



$C_1, C_2, C_3$  canard surface, horizontal only (see fig. 3)

$\frac{\Delta C_n}{\Delta \beta}$  incremental change of yawing-moment coefficient with sideslip angle, per deg

$\frac{\Delta C_l}{\Delta \beta}$  incremental change of rolling-moment coefficient with sideslip angle, per deg

$\frac{\Delta C_Y}{\Delta \beta}$  incremental change of side-force coefficient with sideslip angle, per deg

$C_{N_\alpha}$   $\frac{\partial C_N}{\partial \alpha}$ , slope of the normal-force curve

$C_{m_\alpha}$   $\frac{\partial C_m}{\partial \alpha}$ , static-longitudinal-stability parameter

#### MODEL AND APPARATUS

Sketches of the models are shown in figures 2 and 3, and the geometric characteristics are given in table I. Photographs of various configurations are shown in figure 4. Coordinates for the forebodies of the basic body and the Pilotless Aircraft Research Division (referred to herein as PARD) hypersonic test vehicle are given in table II.

The various configurations were obtained by attaching various combinations of forebodies, flares, and fins to a cylindrical section housing the strain-gage balance.

Four of the configurations (figs. 2(a) to 2(d)) employed a basic body consisting of a five-caliber ogive forebody with a rounded nose having a straight taper to accommodate the canards and a five-caliber cylindrical section. The fins (figs. 2(c) and 2(d)) and canards (fig. 3) were flat plates with rounded leading edges. The fins had blunt trailing edges, whereas the canards had rounded trailing edges. All canards were in the plane of the horizontal fin. Deflections of the canards were set manually.

The hypersonic test vehicle was composed of a five-caliber Von Kármán forebody with a rounded nose, a 5.1 caliber cylindrical section, and a  $10^\circ$  flare (fig. 2(e)).



The models were mounted on a rotary sting to permit testing through ranges of combined angles of attack and sideslip. Six-component force and moment data were measured by an internal strain-gage balance. Base pressures were obtained by averaging the readings of four tubes  $90^\circ$  apart inside the base of the model. Cylindrical wooden blocks approximately the same sizes as the various bases of the models were attached to the sting less than  $1/8$  inch behind the model base to reduce the pressure variation across the base of the model.

## TESTS, CORRECTIONS, AND ACCURACY

### Tests

The tests were made at a Mach number of 2.01, a stagnation temperature of  $100^\circ$  F, and a stagnation pressure of about 1,160 pounds per square foot absolute. The Reynolds number was  $2 \times 10^6$  per foot. Stagnation dewpoints of  $-25^\circ$  or below were maintained to eliminate condensation effects. Tests were made through an angle of attack range of  $0^\circ$  to about  $28^\circ$  at sideslip angles of about  $0^\circ$  and  $4^\circ$ .


### Corrections and Accuracy

Angles of attack and sideslip were corrected for the deflection of the sting and balance under load. The Mach number variation was about  $\pm 0.015$ , and the flow variations in the vertical and horizontal planes did not exceed  $\pm 0.1^\circ$ . No corrections have been applied to the data for these variations.

The axial-force data were adjusted to a base pressure equal to free-stream static pressure. Since the measured base pressures were about the same as test-section static pressure for angles of attack up to about  $8^\circ$ , the wooden block apparently was effective in producing approximately constant pressures across the base of the model.

Probable errors in the force and moment data for small angles of sideslip are considerably larger for the body configurations without fins than for the body-fin configurations because the strain-gage balance was not able to measure very small loads with sufficient accuracy. Small increments of forces and moments could be accurately measured in the higher load ranges.

Estimated probable errors in the force and moment data based on the repeatability of the results, zero shift, calibration, and random instrument errors are as follows:



$C_N$	.....	$\pm 0.034$
$C_A$	.....	$\pm 0.002$
$C_m$	.....	$\pm 0.099$
$C_z$	.....	$\pm 0.005$
$C_n$	.....	$\pm 0.099$
$C_Y$	.....	$\pm 0.032$

The angles of attack at zero sideslip and the sideslip angles at zero angle of attack are estimated to be correct to within  $\pm 0.1^\circ$ . For combined angles of attack and sideslip the angles are correct to within  $\pm 0.2^\circ$ . Deflection angles of the canards are correct to within  $\pm 0.1^\circ$ .

## RESULTS AND DISCUSSION

### Longitudinal Stability

Effects of afterbody flare.- The effects of afterbody flare on the aerodynamic characteristics in pitch are shown in figure 5. It should be noted that the hypersonic test vehicle has a slightly different nose and a smaller flare than the body with the  $10^\circ$  flare configuration (fig. 2). The addition of the  $10^\circ$  flare to the body resulted in higher normal forces, increased longitudinal stability  $-C_{m_\alpha}$ , and large increments of axial force  $C_A$ . The lower values of  $C_{m_\alpha}$  and  $C_A$  indicated for the hypersonic test vehicle are probably caused by the smaller flare, although the increments in normal force were about the same as those for the body with the  $10^\circ$  flare. The normal-force and pitching-moment characteristics were very nonlinear and indicated a progressive increase in  $C_{N_\alpha}$  and  $-C_{m_\alpha}$  with increasing angle of attack.

Effects of fin plan form.- The addition of fins to the body resulted in increases in longitudinal stability, slope of the normal-force curve, and axial forces, with the larger fins ( $5^\circ$ ) providing the greater increases (fig. 6). The addition of either the  $15^\circ$  fins or the  $10^\circ$  flare to the body resulted in about the same increments of  $C_N$  (figs. 5 and 6), although the body with  $15^\circ$  fins had considerably lower values of axial force and a more nearly linear variation of  $C_m$  with  $\alpha$ .

Effect of canard plan form.- The effects of canard plan form for zero canard deflection on the aerodynamic characteristics in pitch of the body with  $5^\circ$  fins are presented in figure 7. All of the canards resulted in a decrease in the level of longitudinal stability and provided net

increases in normal force. Larger positive increments of  $C_m$  and slightly higher values of  $C_N$  were obtained with  $C_3$  than with  $C_2$ . These results are probably caused by the higher aspect ratio and more forward center of pressure of  $C_3$ , although both canards had about the same area. The configuration employing  $C_3$  was unstable near zero angle of attack but at higher angles of attack had about the same level of stability as the other canard configurations. The larger increments of  $C_A$  produced by  $C_3$  might be expected since  $C_3$  had a considerably larger frontal area than  $C_1$  and  $C_2$  (fig. 3).

### Longitudinal-Control Characteristics

The longitudinal-control characteristics for the various configurations are presented in figures 8 to 10. It should be noted that these control characteristics are for a constant center-of-gravity location and not for a constant level of longitudinal stability.

In general, all of the canards were effective pitch controls. Deflection of the canard for each configuration produced a net increase in the values of  $C_N$  and positive increments of  $C_m$  throughout the angle-of-attack range. As the angle of attack increased, the effectiveness of canard deflection in producing  $C_N$  and  $C_m$  decreased.

For the range of canard deflections tested, the body with  $15^\circ$  fins and  $C_1$  had a more nearly linear pitching-moment variation with angle of attack and smaller values of axial force than any other tested configuration (fig. 9). However, because of the higher values of normal force available, any of the configurations employing the  $5^\circ$  fins should be capable of greater normal accelerations than configurations with either the  $15^\circ$  fins or the  $10^\circ$  flare. The largest increments of  $C_m$  and the highest values of  $C_N$  were obtained through the use of  $C_3$  with the body and  $5^\circ$  fins (fig. 10(c)), but the variation of  $C_m$  with  $\alpha$  was nonlinear.

### Lateral Stability

The values of the sideslip characteristics  $\frac{\Delta C_n}{\Delta \beta}$ ,  $\frac{\Delta C_l}{\Delta \beta}$ , and  $\frac{\Delta C_y}{\Delta \beta}$  were obtained from tests in which the sideslip angle was held constant at about  $0^\circ$  and  $4^\circ$  while the angle of attack was varied.



Effects of afterbody flare.- The addition of the  $10^\circ$  flare to the body provided negative increments of side force and positive increments of yawing moment such that the body with the  $10^\circ$  flare was directionally stable throughout the angle-of-attack range (fig. 11). Similar characteristics were indicated for the hypersonic test vehicle, although the levels of  $-\frac{\Delta C_Y}{\Delta \beta}$  and  $\frac{\Delta C_n}{\Delta \beta}$  were lower than for the body with the  $10^\circ$  flare. No indications of induced roll effects were obtained for any of the configurations for the angle-of-attack range investigated.

Effects of fin plan form.- The addition of the  $5^\circ$  or  $15^\circ$  fins produced directional stability throughout the angle-of-attack range (fig. 12). The  $5^\circ$  fins provided only slightly larger values of  $\frac{\Delta C_n}{\Delta \beta}$  but considerably higher values of  $-\frac{\Delta C_Y}{\Delta \beta}$  than the  $15^\circ$  fins, therefore, a more forward center-of-pressure location was indicated. Induced roll effects were indicated for both configurations for angles of attack greater than  $8^\circ$ .

Effect of canard plan form.- The effects of canard plan form on the sideslip characteristics of the body with  $5^\circ$  fins at zero canard deflection are presented in figure 13. The variations of  $\frac{\Delta C_n}{\Delta \beta}$  and  $\frac{\Delta C_Y}{\Delta \beta}$  for the various canard configurations indicate that at the lower angles of attack the canard probably reduces the fin effectiveness. However, at higher angles the canard probably diminishes the destabilizing forces on the forebody and has a less adverse effect on the fins.

The addition of  $C_1$  or  $C_3$  did not greatly alter the values of effective dihedral for the body-fin configuration. Large increments of negative effective dihedral were obtained at the higher angles of attack for the body with  $5^\circ$  fins and  $C_2$  configuration.

Effects of canard deflection.- The effects of canard deflection on the sideslip characteristics of the various configurations are presented in figures 14 to 16. Deflection of the canards generally increased the magnitude of the effects on the directional stability and side force that resulted from adding the canards at zero deflection to the body-fin configurations (fig. 13). Large variations in effective dihedral  $\frac{\Delta C_l}{\Delta \beta}$  with canard deflection were obtained. These variations ranged from no effect for the body with the  $10^\circ$  flare and  $C_1$  configuration (fig. 14) to significant variations in effective dihedral over most of the angle-of-attack range for the body with fins. These changes in the rolling-moment characteristics with canard deflection apparently result from interference effects of the various canards on the fins.



An inspection of additional results obtained in combined pitch and sideslip indicate large interference effects on pitching moment, yawing moment, and normal force.

### CONCLUSIONS

The investigation of several hypersonic missile configurations and various canard controls for combined angles of attack and sideslip at a Mach number of 2.01 with the moment center at the 50-percent body station has indicated the following conclusions:

1. The addition of a flared afterbody or either set of cruciform fins resulted in longitudinally stable configurations, but the body with the  $5^\circ$  fins should be capable of producing the largest normal accelerations.
2. The canards were effective longitudinal controls producing positive increments of normal force and pitching moment which progressively decreased with increasing angle of attack.
3. The addition of the flared afterbody or the cruciform fins provided directional stability throughout the angle-of-attack range.
4. The addition or deflection of the canards decreased the directional stability at low angles of attack but had a stabilizing effect at higher angles.
5. The canards caused significant induced rolling moments for the cruciform fin configurations but not for the flared afterbody configuration.

Langley Aeronautical Laboratory,  
National Advisory Committee for Aeronautics,  
Langley Field, Va., January 6, 1958.



## REFERENCES

1. Robinson, Ross B.: Aerodynamic Characteristics of Missile Configuration With Wings of Low Aspect Ratio for Various Combinations of Forebodies, Afterbodies, and Nose Shapes for Combined Angles of Attack and Sideslip at a Mach Number of 2.01. NACA RM L57D19, 1957.
2. Katzen, Elliott D., and Jorgensen, Leland H.: Aerodynamics of Missiles Employing Wings of Very Low Aspect Ratio. NACA RM A55L13b, 1956.
3. Jorgensen, Leland H., and Katzen, Elliott D.: Wing-Body Combinations With Wings of Very Low Aspect Ratio at Supersonic Speeds. NACA RM A56G16, 1956.
4. Bland, William M., Jr., and Kolenkiewicz, Ronald: Free-Flight Pressure Measurements Over a Flare-Stabilized Rocket Model With a Modified Von Kármán Nose for Mach Numbers up to 4.3. NACA RM L57J24, 1957.

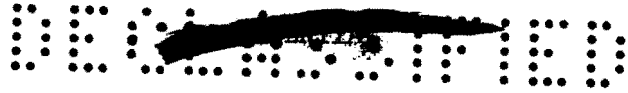


TABLE I

MODEL DIMENSIONS

Body :

Length, in. . . . .	30.00
Diameter, in. . . . .	3.00
Cross-sectional area, sq in. . . . .	7.07
Fineness ratio of nose . . . . .	5.00
Length-diameter ratio . . . . .	10.00
Moment center location, percent length . . . . .	50.0

10° flare :

Length, in. . . . .	6.01
Base diameter, in. . . . .	5.13
Base area, sq in. . . . .	20.66

Fins:

	<u>5°</u>	<u>15°</u>
Area, exposed, 2 fins, sq in. . . . .	34.36	9.55
Root chord, in. . . . .	19.12	5.97
Tip chord, in. . . . .	0	0
Span, exposed, 2 fins, in. . . . .	3.20	3.20
Span, total, 2 fins, in. . . . .	6.20	6.20
Taper ratio . . . . .	0	0
Aspect ratio, exposed . . . . .	0.268	1.072
Span diameter ratio . . . . .	2.07	2.07
Leading edge sweep, deg . . . . .	85	75

Hypersonic test vehicle:

Length, in. . . . .	35.11
Diameter, in. . . . .	3.00
Cross-sectional area, sq in. . . . .	7.07
Fineness ratio of nose . . . . .	5.00
Length-diameter ratio . . . . .	11.70
Flare angle, deg . . . . .	10.0
Base area, sq in. . . . .	16.91
Moment center location, percent length . . . . .	50.0

Canards:

	<u>c<sub>1</sub></u>	<u>c<sub>2</sub></u>	<u>c<sub>3</sub></u>
Area, exposed, sq in. . . . .	5.20	7.76	7.88
Span, total in. . . . .	3.00	3.00	4.86
Leading edge sweep angle, deg . . . . .	45.0	45.0	45.0
Area ratio (to 5° fins). . . . .	0.15	0.23	0.23
Area ratio (to 15° fins) . . . . .	0.54	0.81	0.82



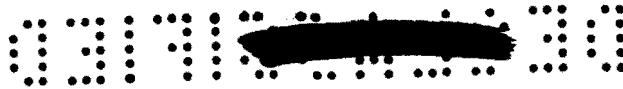


TABLE II

## FOREBODY COORDINATES

Basic body		Hypersonic test vehicle	
x, in.	R, in.	x, in.	R, in.
0	0	0	0
.30	.300	.054	.054
6.00	.963	1.424	.299
7.00	1.073	1.673	.342
8.00	1.176	2.174	.423
9.00	1.262	2.672	.495
10.00	1.335	3.173	.564
11.00	1.394	3.419	.600
12.00	1.441	3.671	.630
13.00	1.474	4.172	.693
14.00	1.493	4.673	.753
15.00	1.500	4.802	.768
		6.170	.918
		7.670	1.059
		9.170	1.188
		10.670	1.296
		12.179	1.389
		13.670	1.461
		15.170	1.500

Note: Sta.  $x = 0.30$  to  $x = 6.00$  is a straight taper.



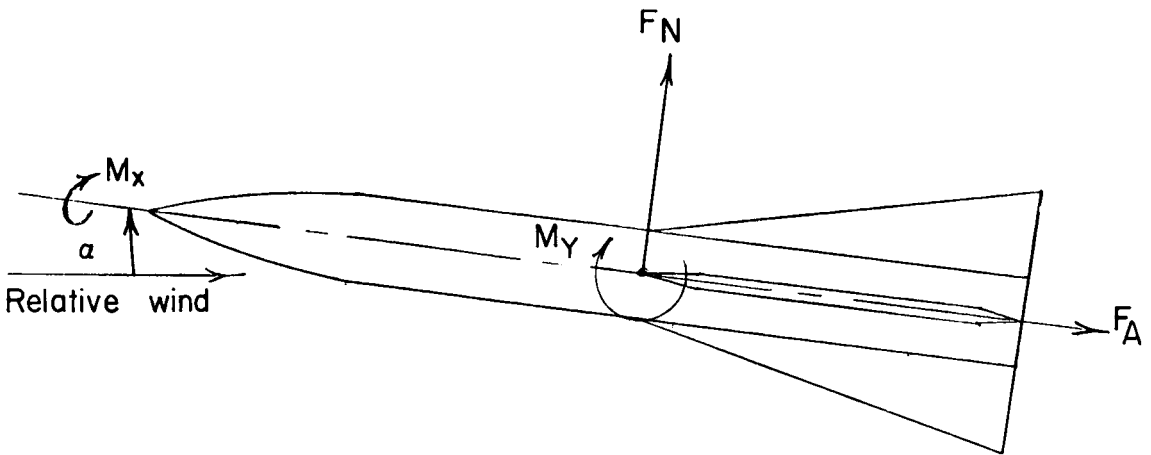
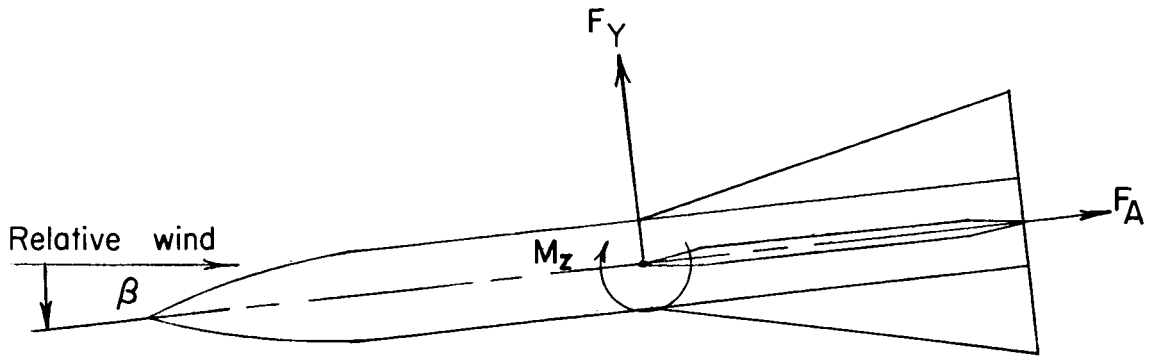
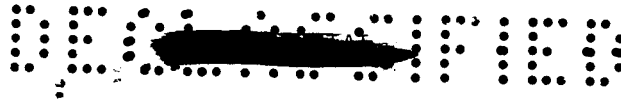
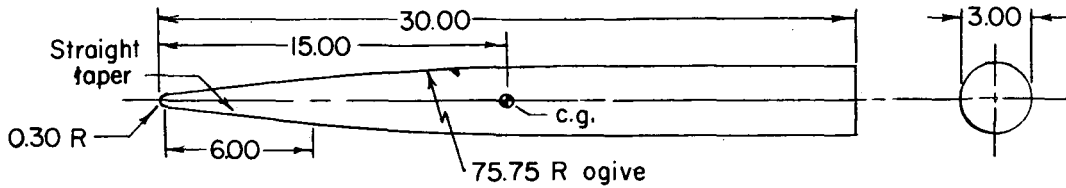
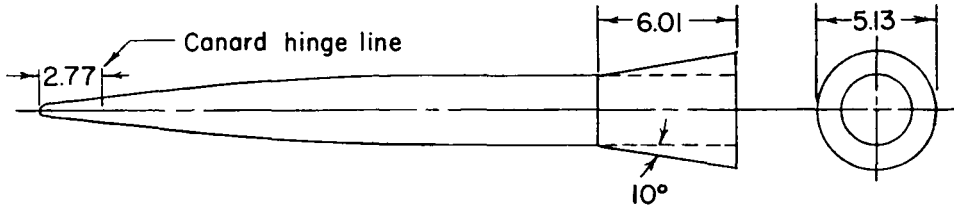


Figure 1.- Body-axis system. Arrows indicate positive directions of forces, moments, and angles.

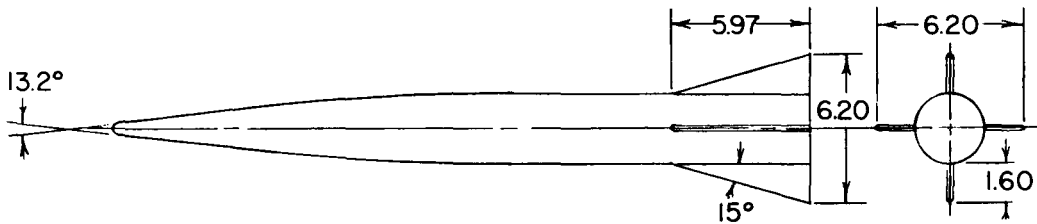




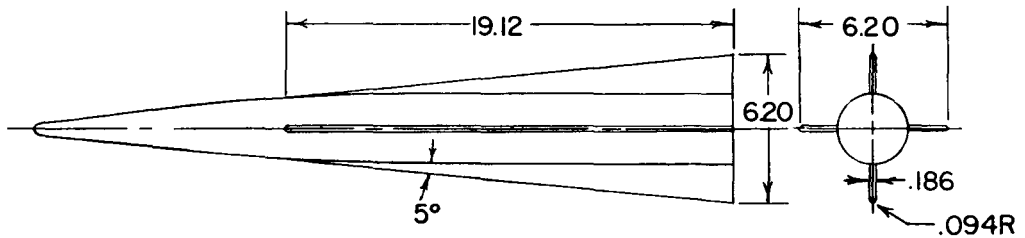
(a) Basic body.



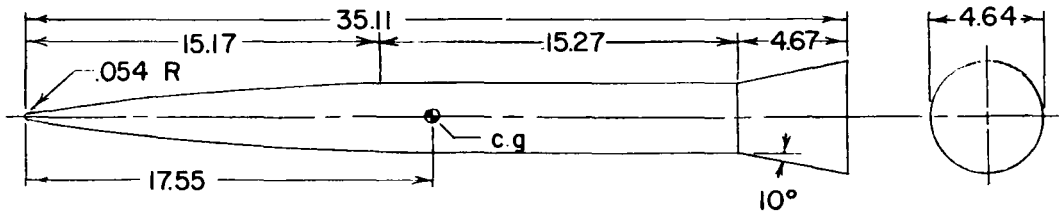
(b) Body with 10° flare.



(c) Body with 15° fins.



(d) Body with 5° fins.



(e) PARD hypersonic test vehicle.

Figure 2.- Sketches of models. Linear dimensions are in inches.

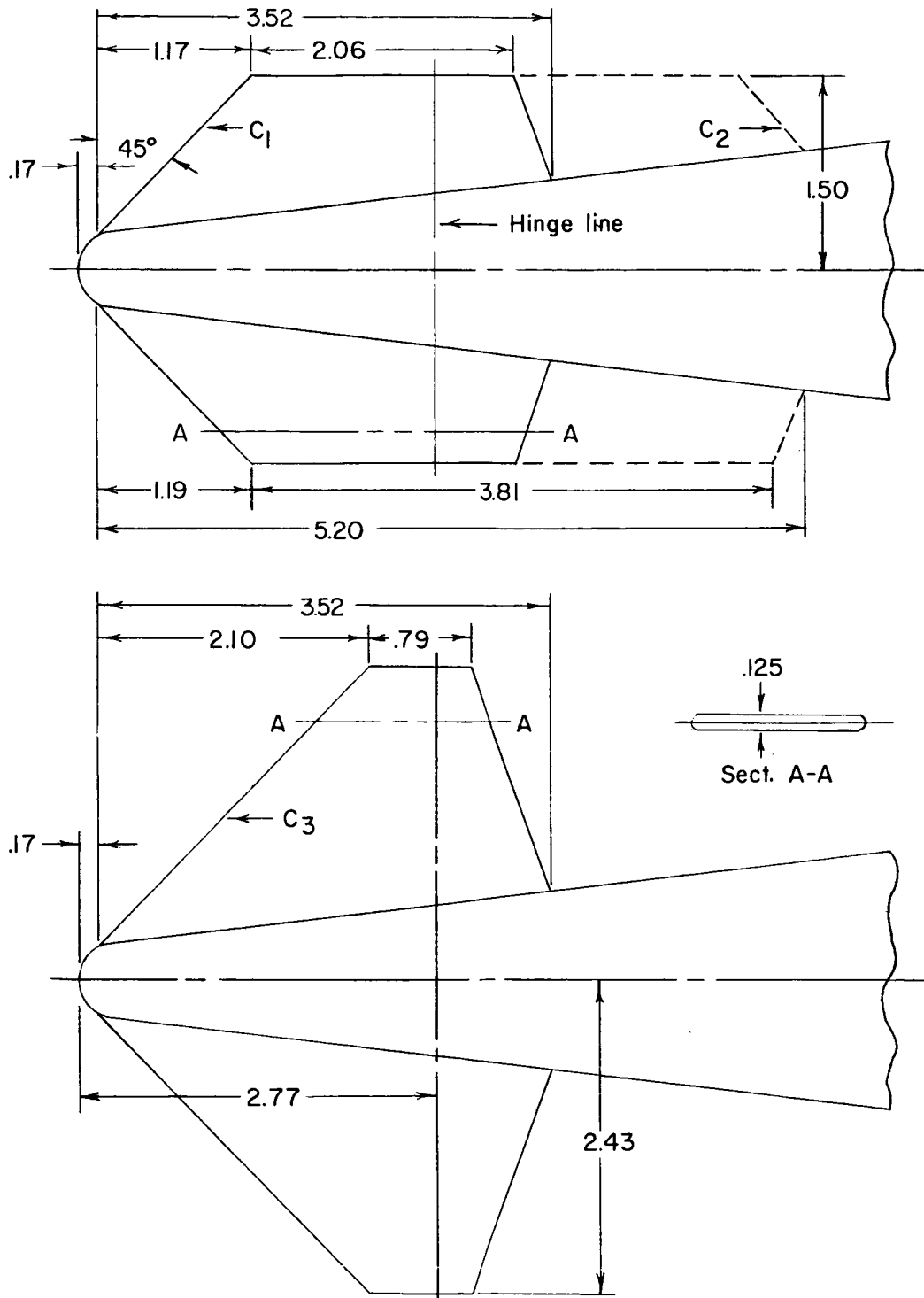
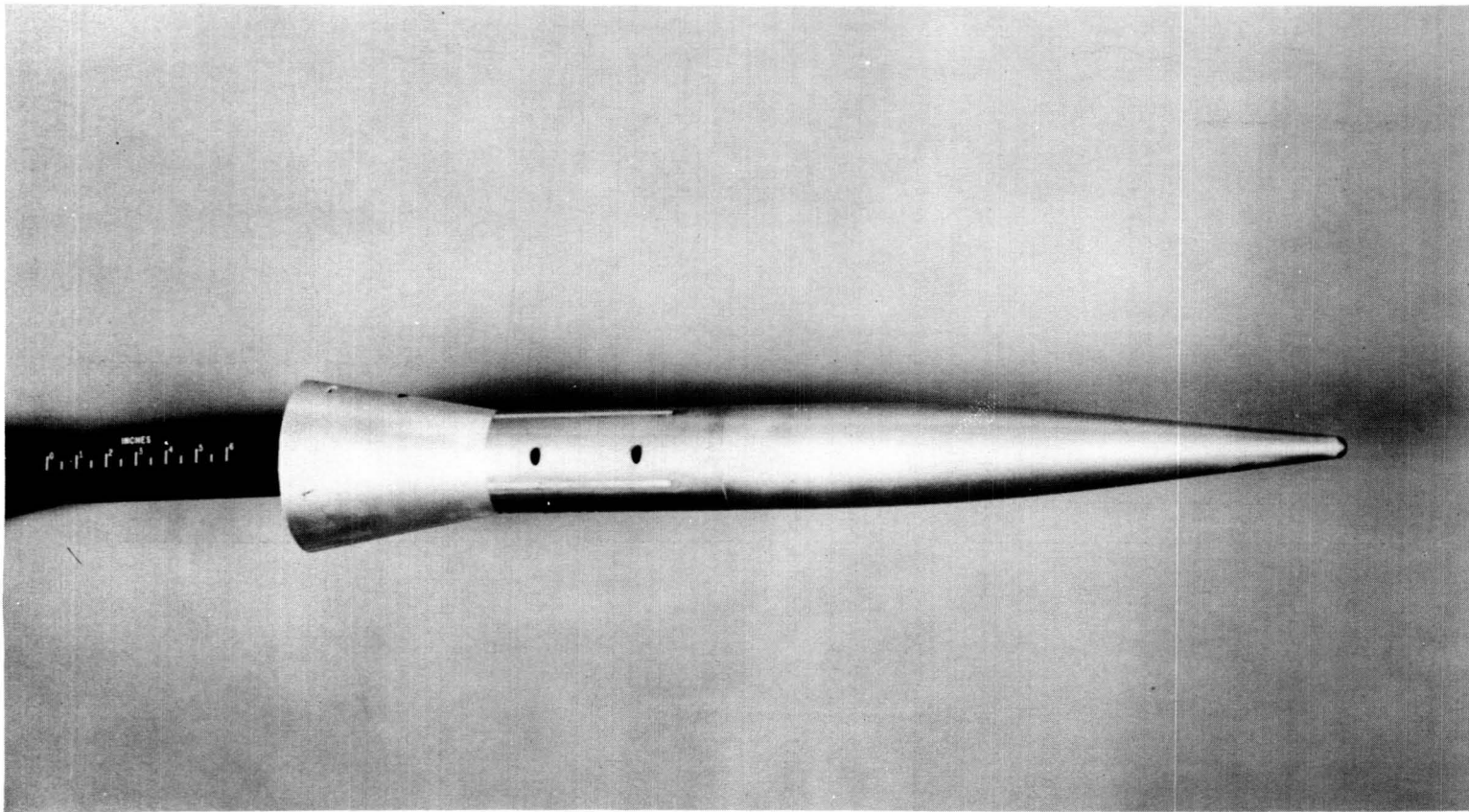


Figure 3.- Details of canards. Linear dimensions are in inches.



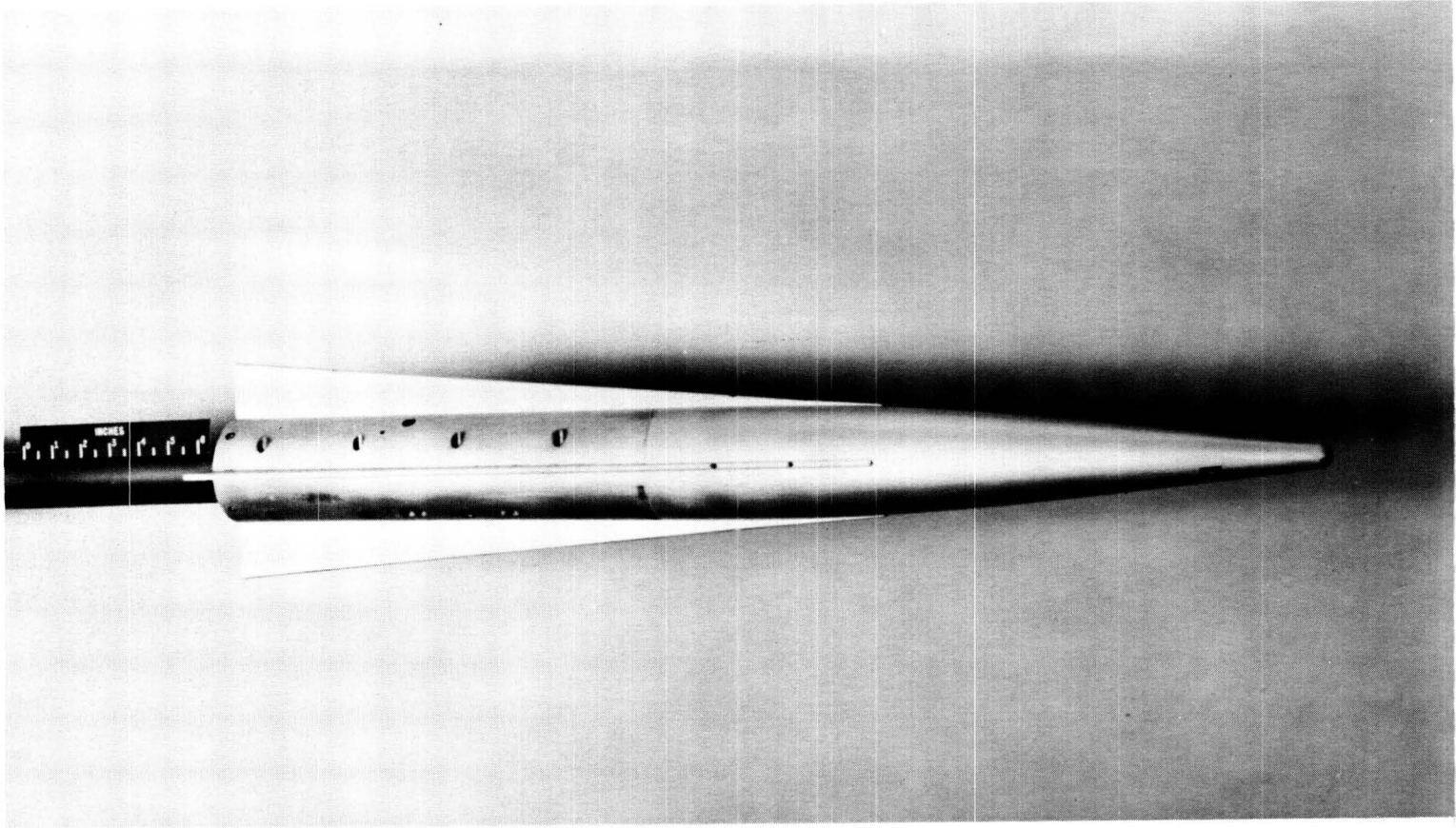




(a) Body with  $10^\circ$  flare.

L-57-2412

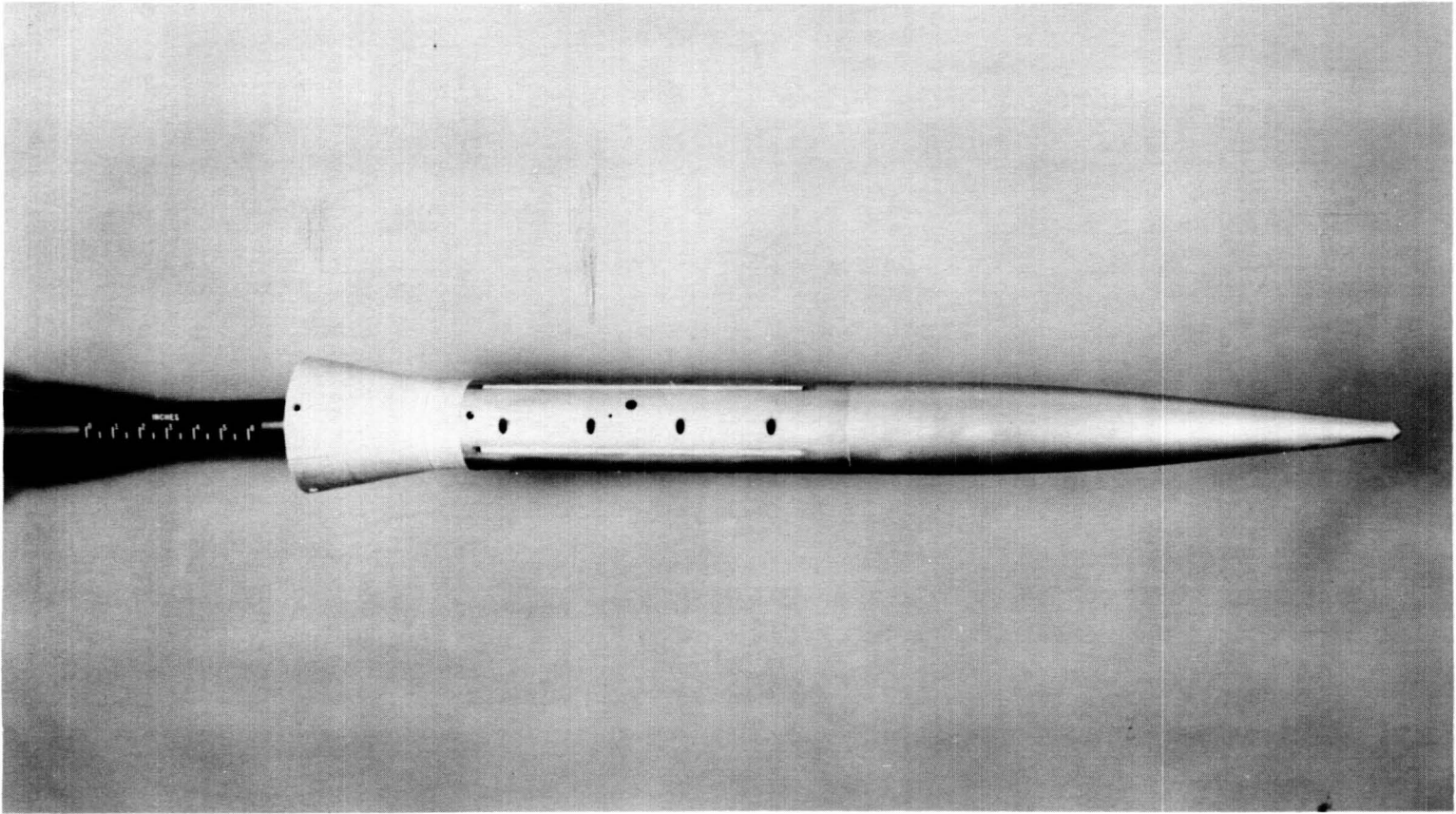
Figure 4.- Photographs of models.



(b) Body with  $5^\circ$  fins.

L-57-2414

Figure 4.- Continued.



(c) Hypersonic test vehicle.

L-57-2411

Figure 4.- Concluded.



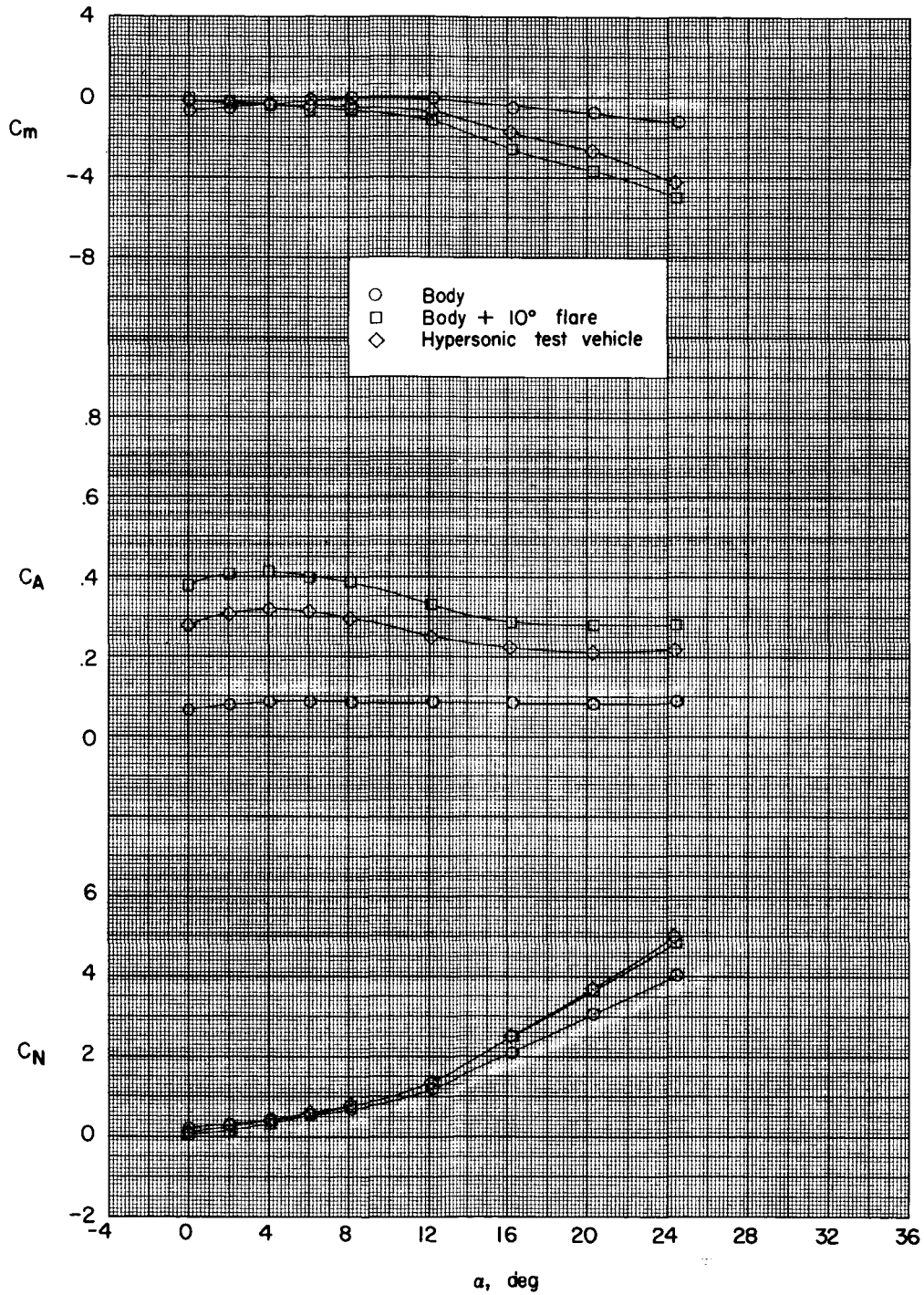


Figure 5.- Effects of afterbody flare on the aerodynamic characteristics in pitch.

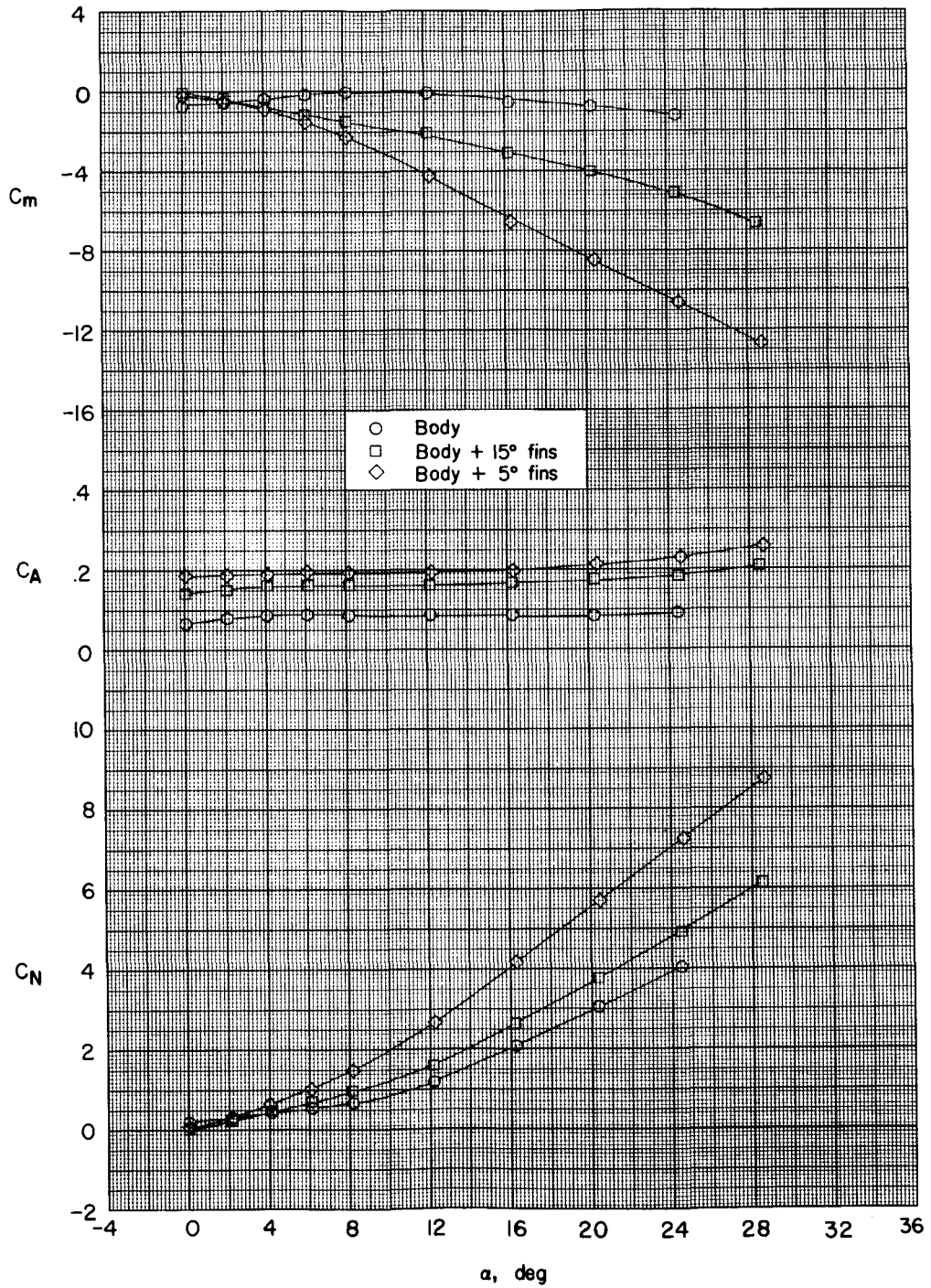


Figure 6.- Effect of fin plan form on the aerodynamic characteristics in pitch.

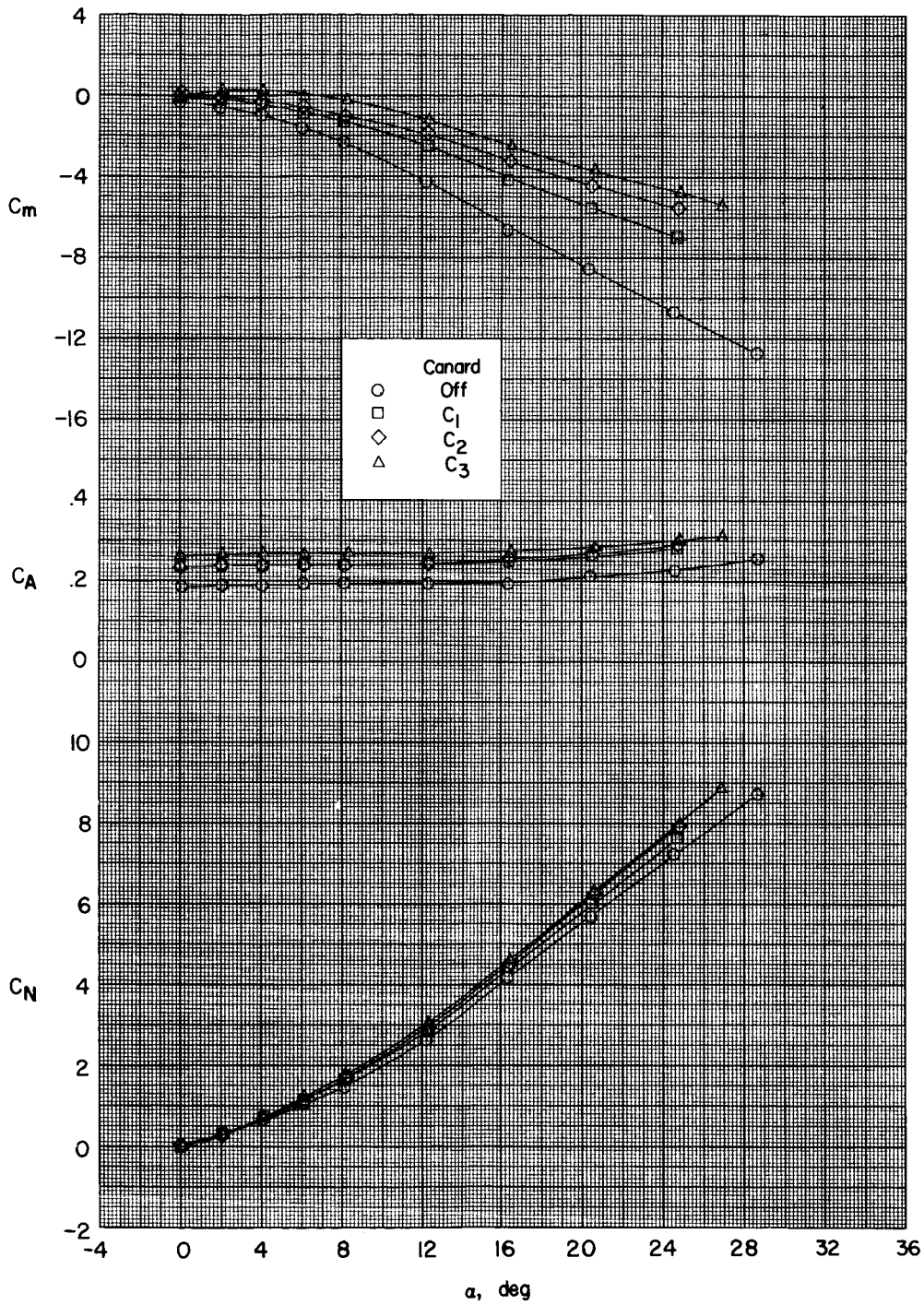


Figure 7.- Effect of canard plan form on the aerodynamic characteristics in pitch. Body with  $5^\circ$  fins;  $\delta_c = 0^\circ$ .

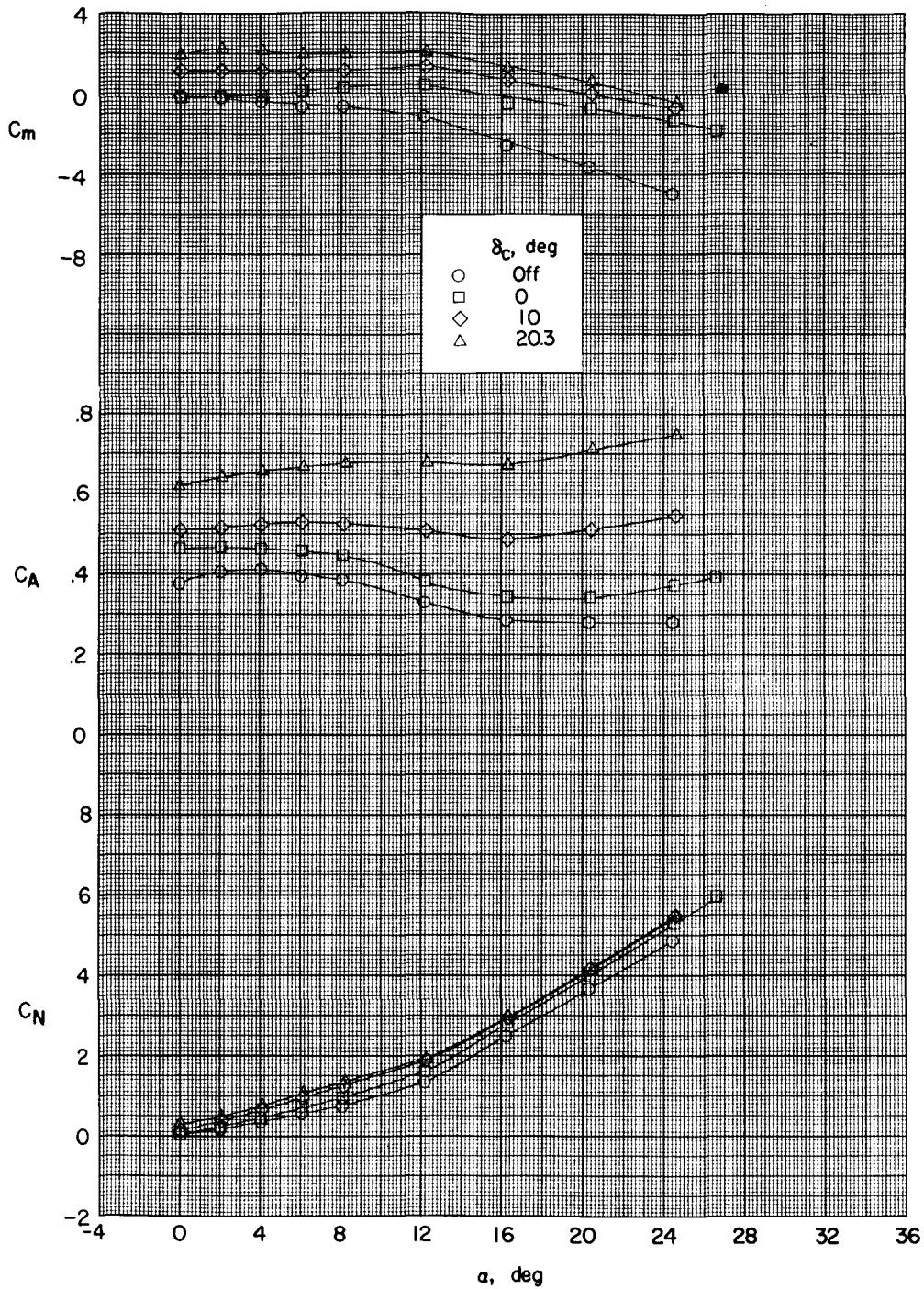


Figure 8.- Effect of canard deflection on the aerodynamic characteristics in pitch of the body with  $10^\circ$  flare and  $C_1$  configuration.

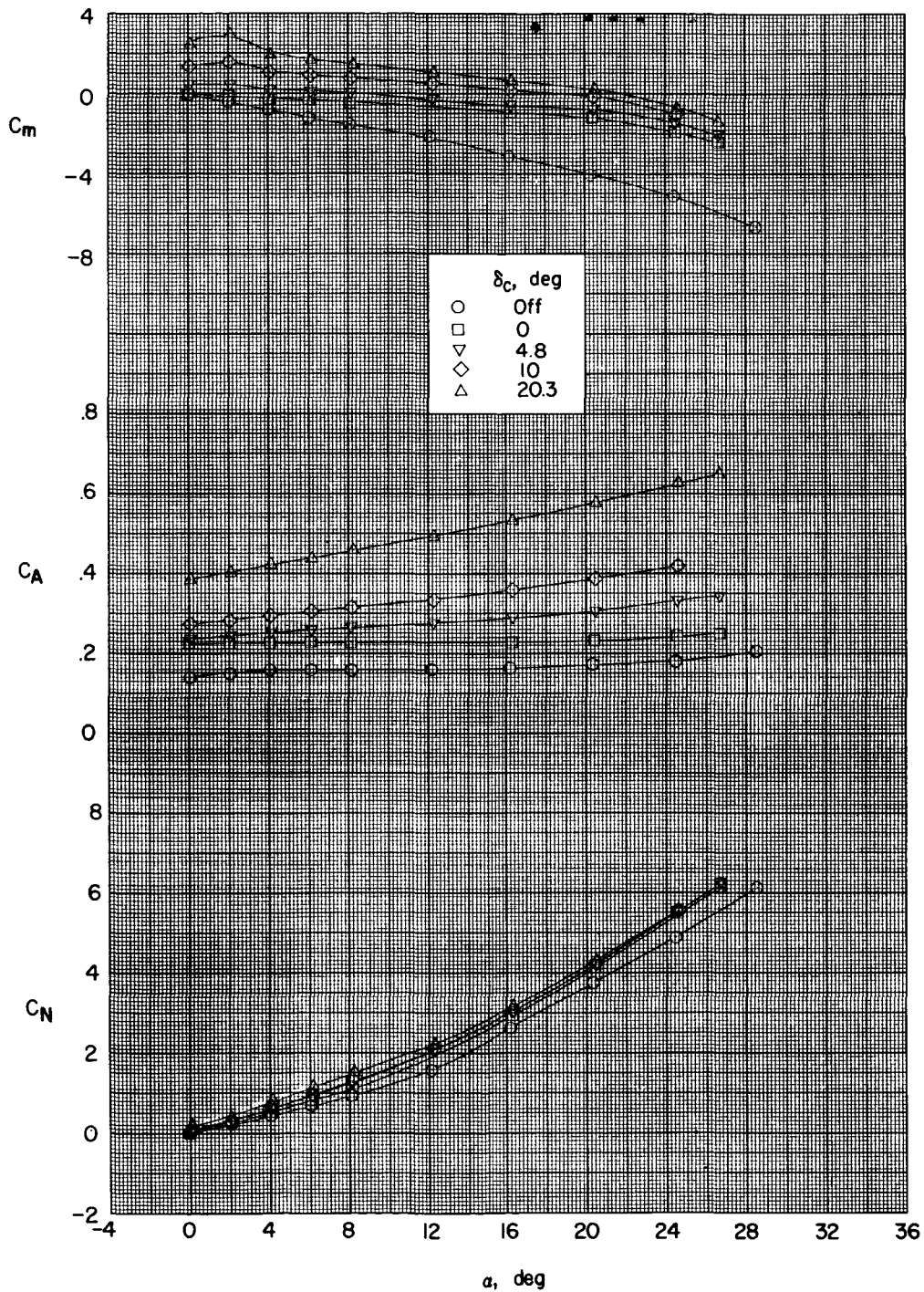
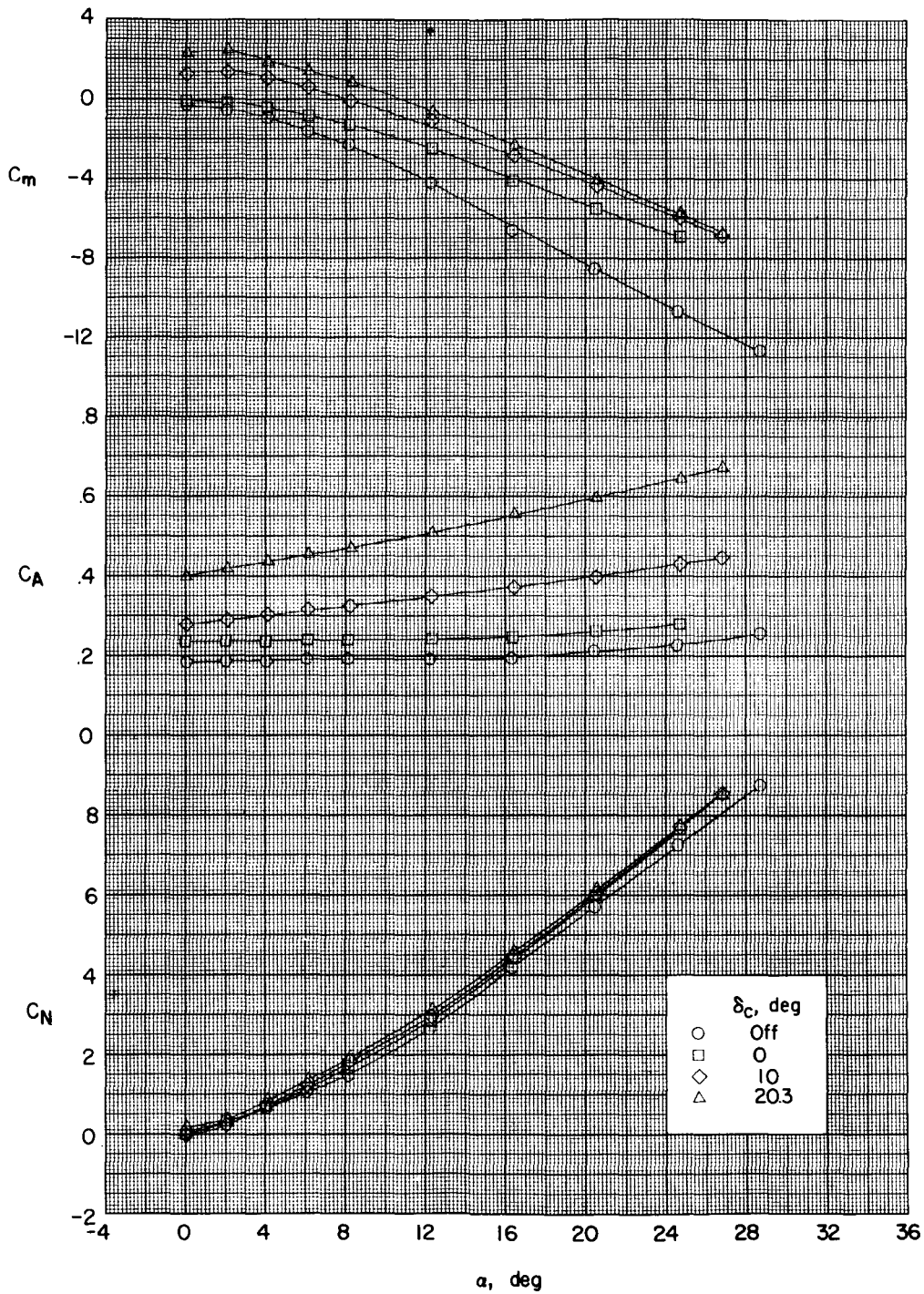


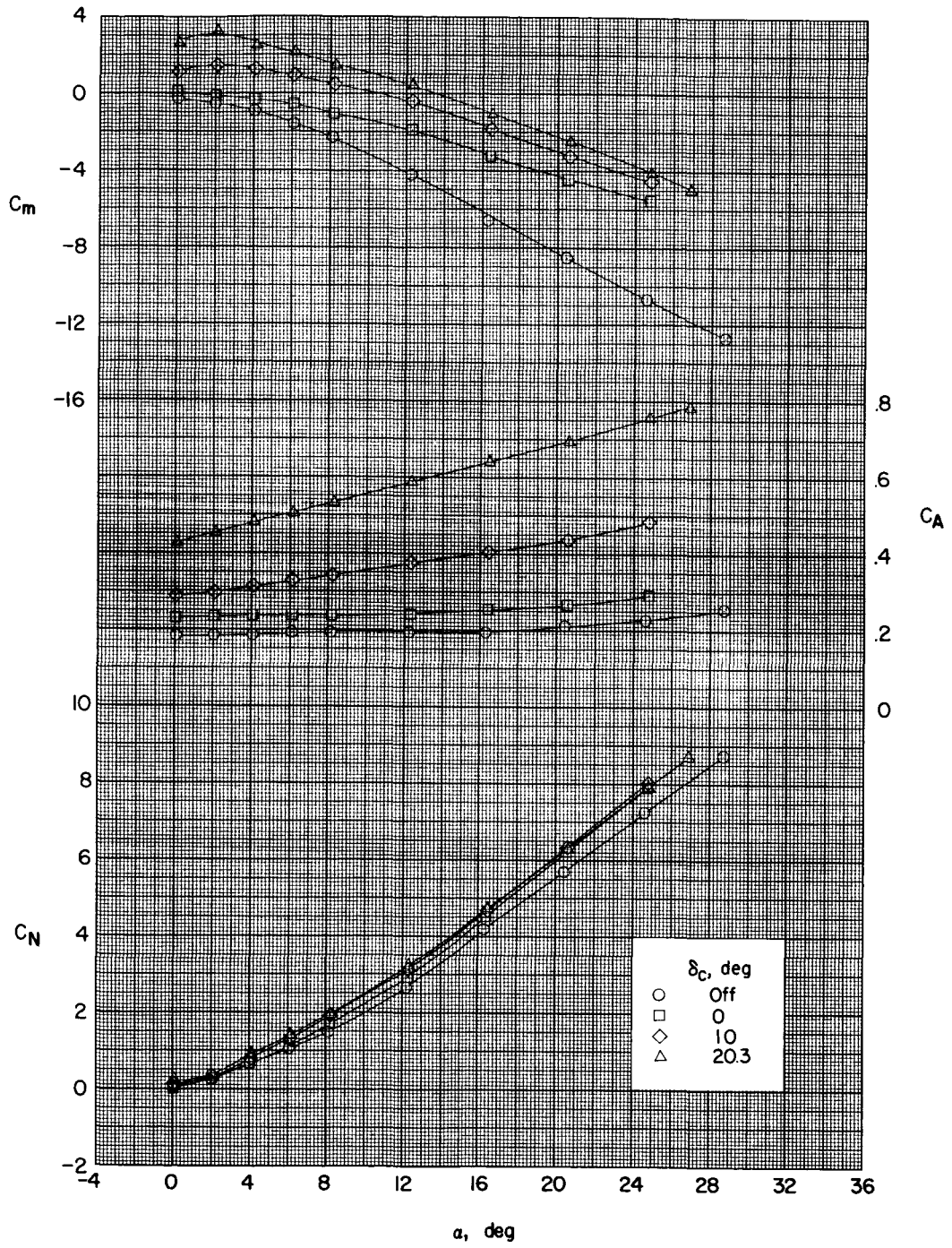
Figure 9.- Effect of canard deflection on the aerodynamic characteristics in pitch of the body with  $15^\circ$  fins and  $C_1$  configuration.





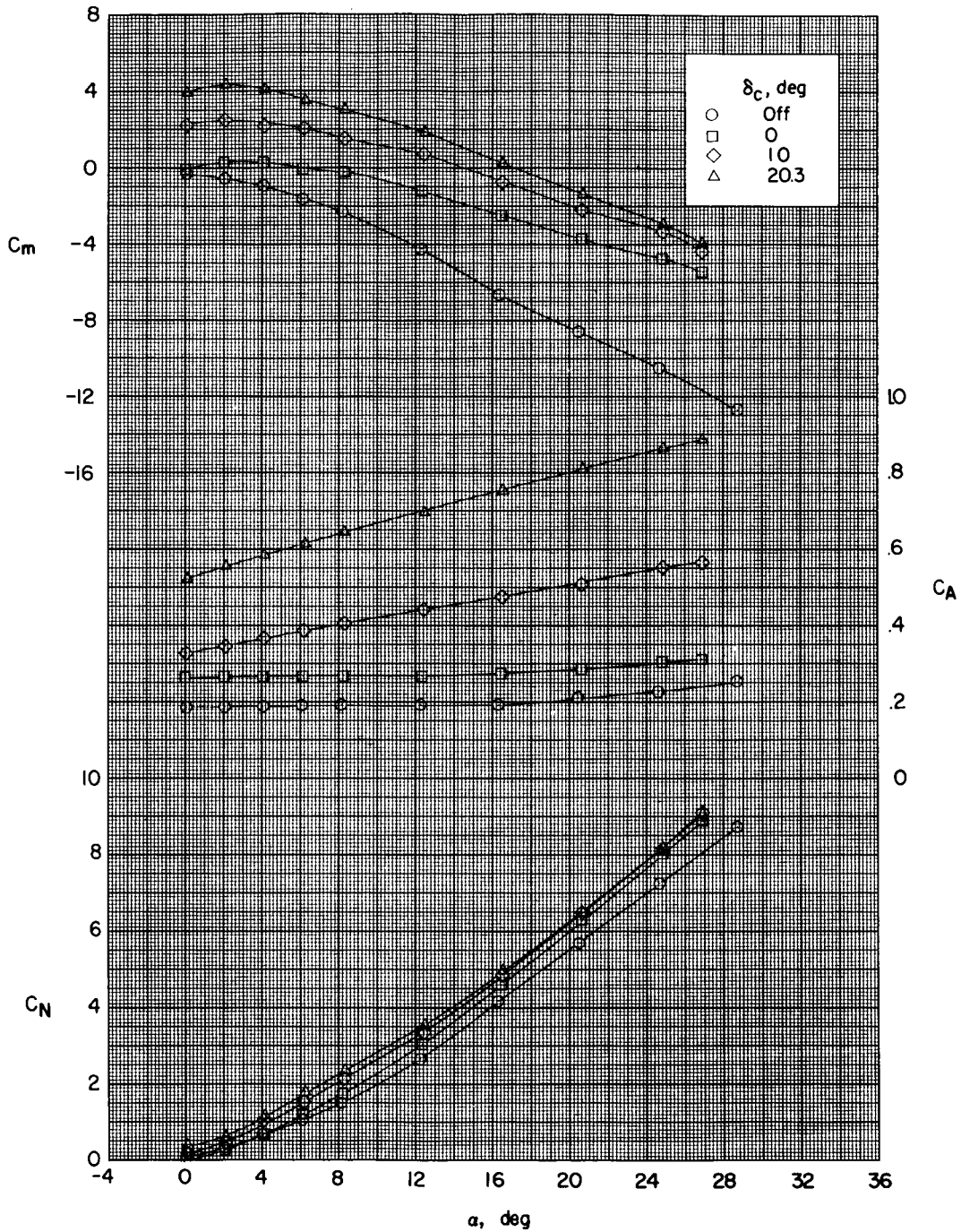
(a)  $C_1$ .

Figure 10.- Effects of canard deflection on the aerodynamic characteristics in pitch for the body with 5° fins configuration with various canards.



(b)  $C_2$ .

Figure 10.- Continued.



(c)  $C_3$ .

Figure 10.- Concluded.



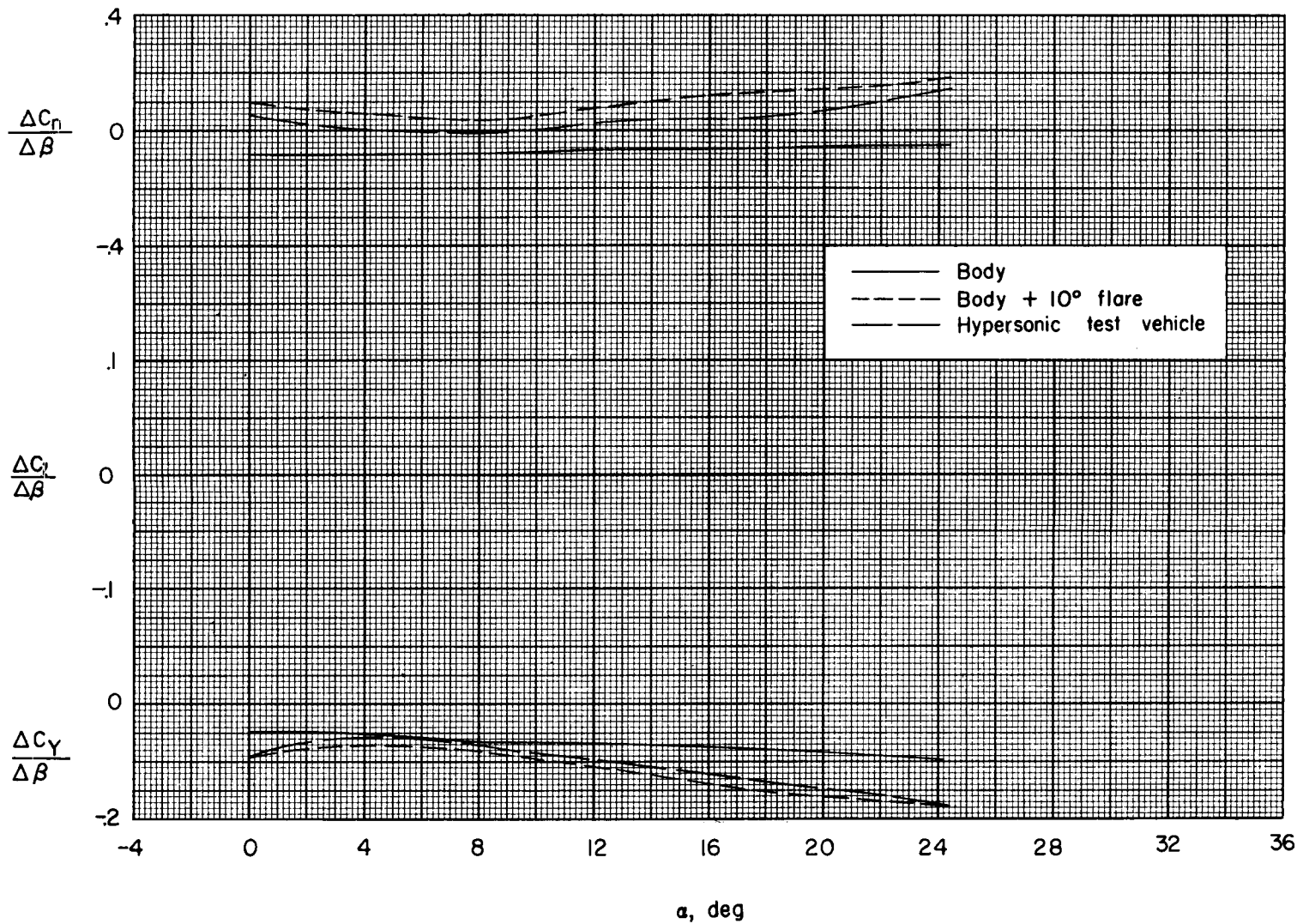


Figure 11.- Effect of afterbody flare on the sideslip characteristics.

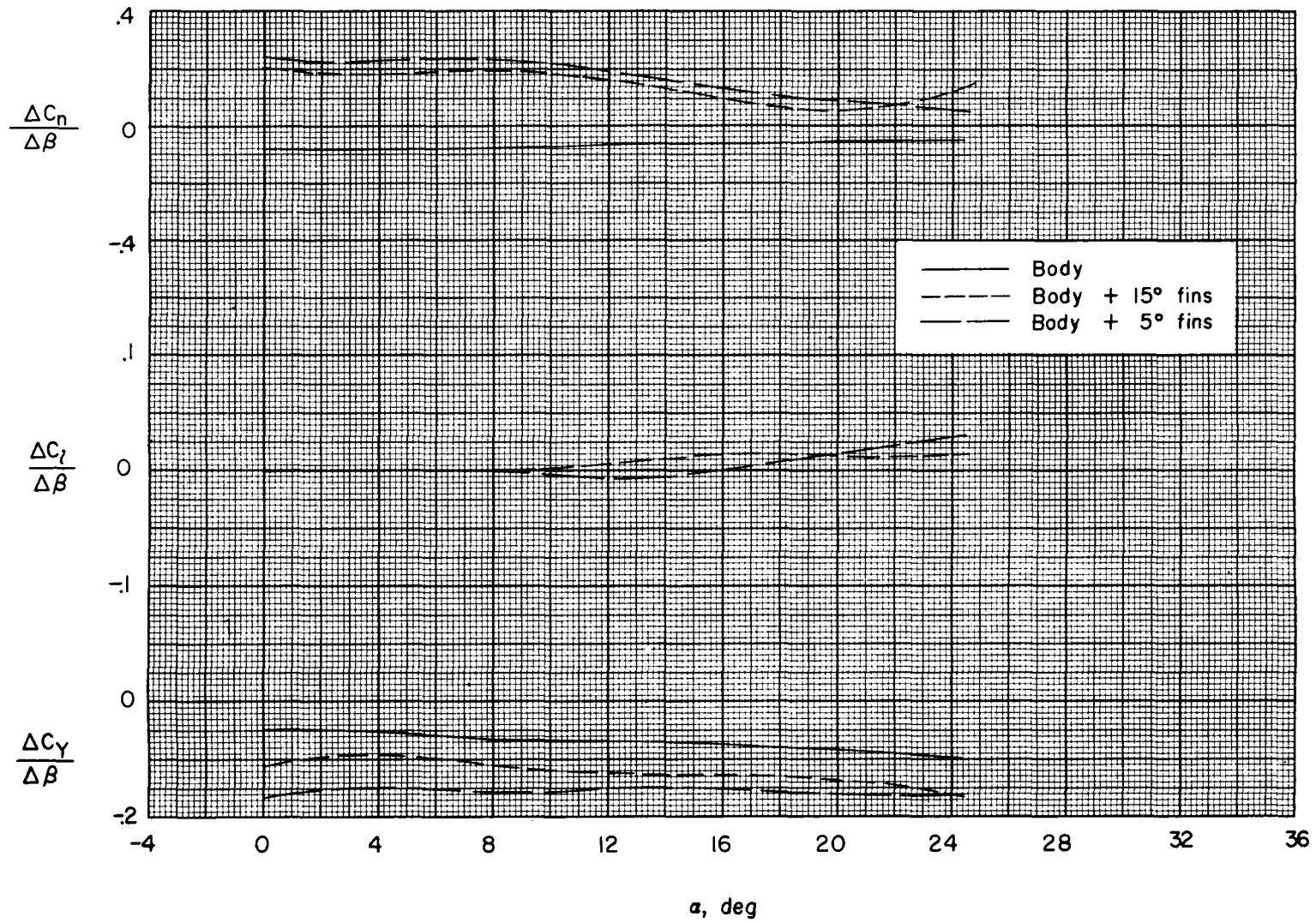


Figure 12.- Effects of fin plan form on the sideslip characteristics.

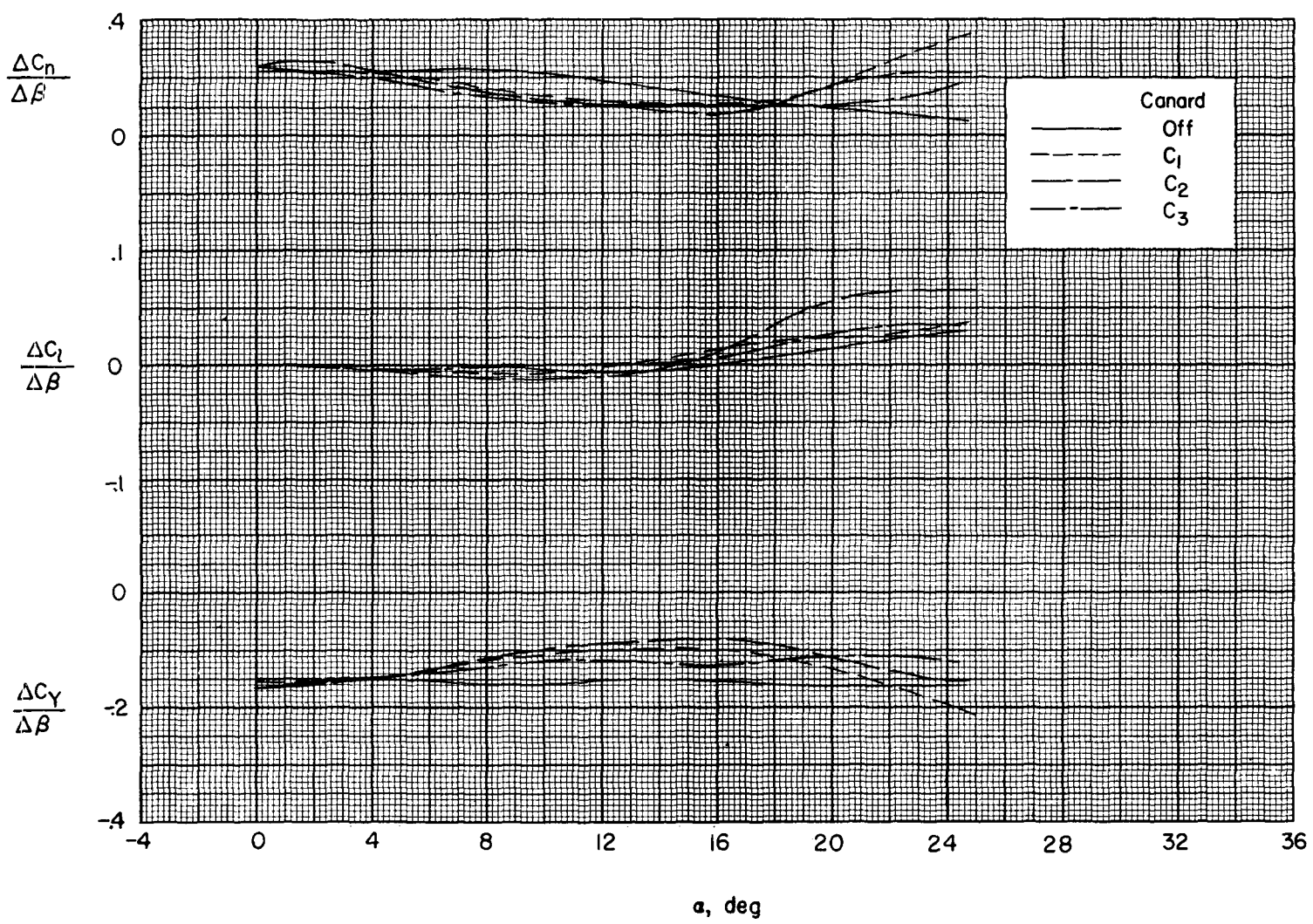


Figure 13.- Effect of canard plan form on the sideslip characteristics. Body with  $5^\circ$  fins;  $\delta_c = 0^\circ$ .

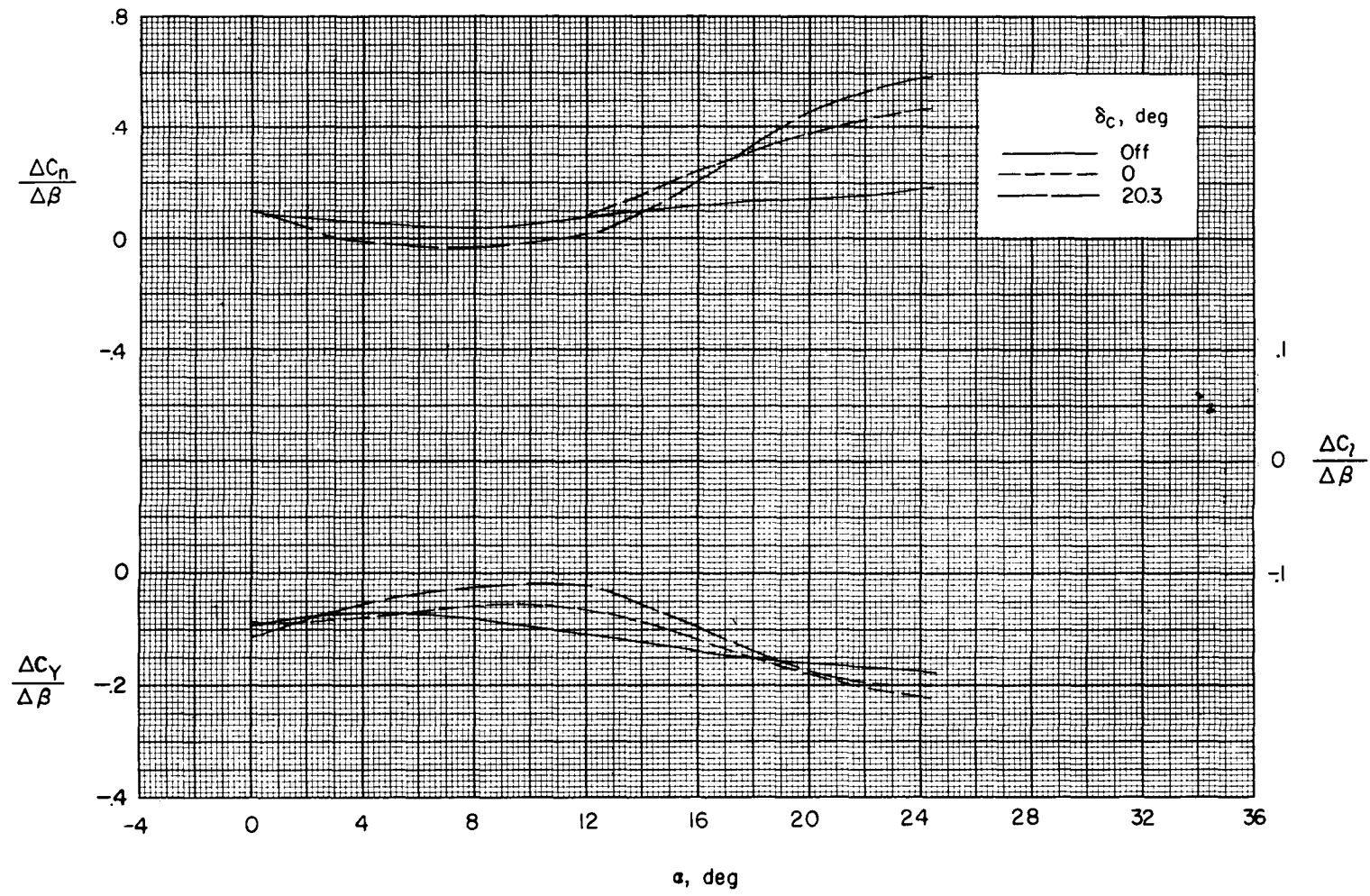


Figure 14.- Effect of canard deflection on the sideslip characteristics for the body with 10° flare and C<sub>1</sub> configuration.

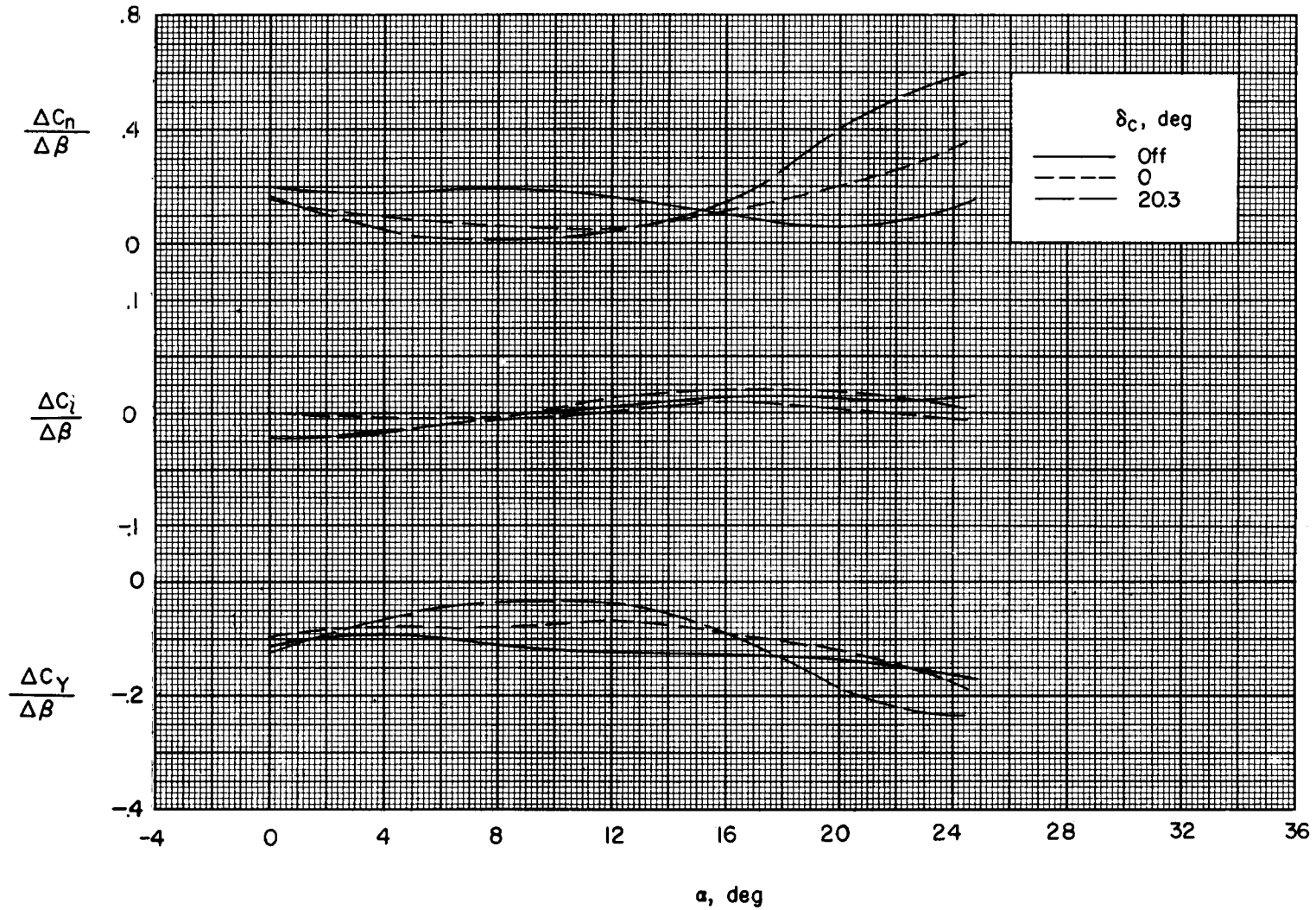


Figure 15.- Effect of canard deflection on the sideslip characteristics for the body with 15° fins and  $C_1$  configuration.



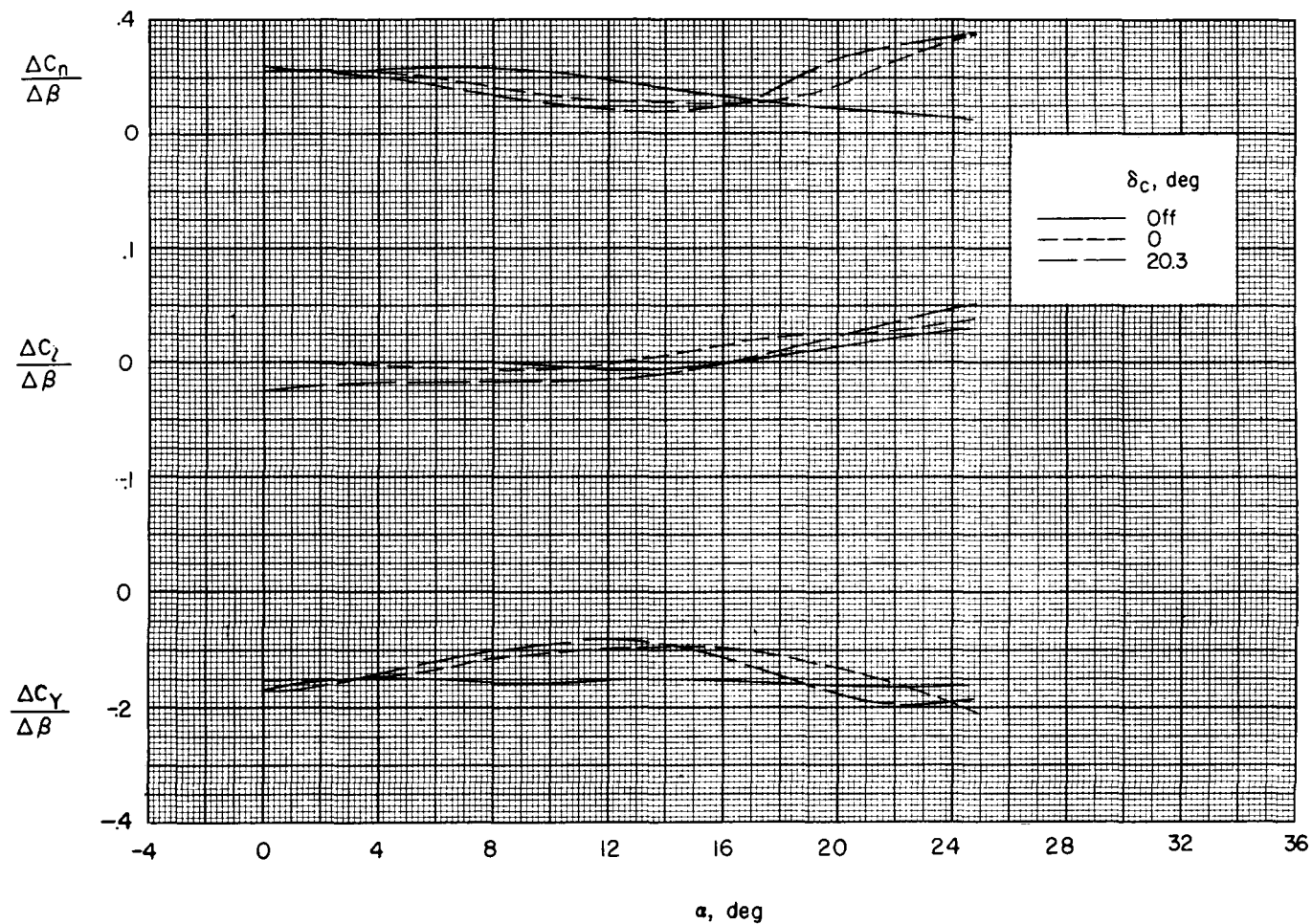
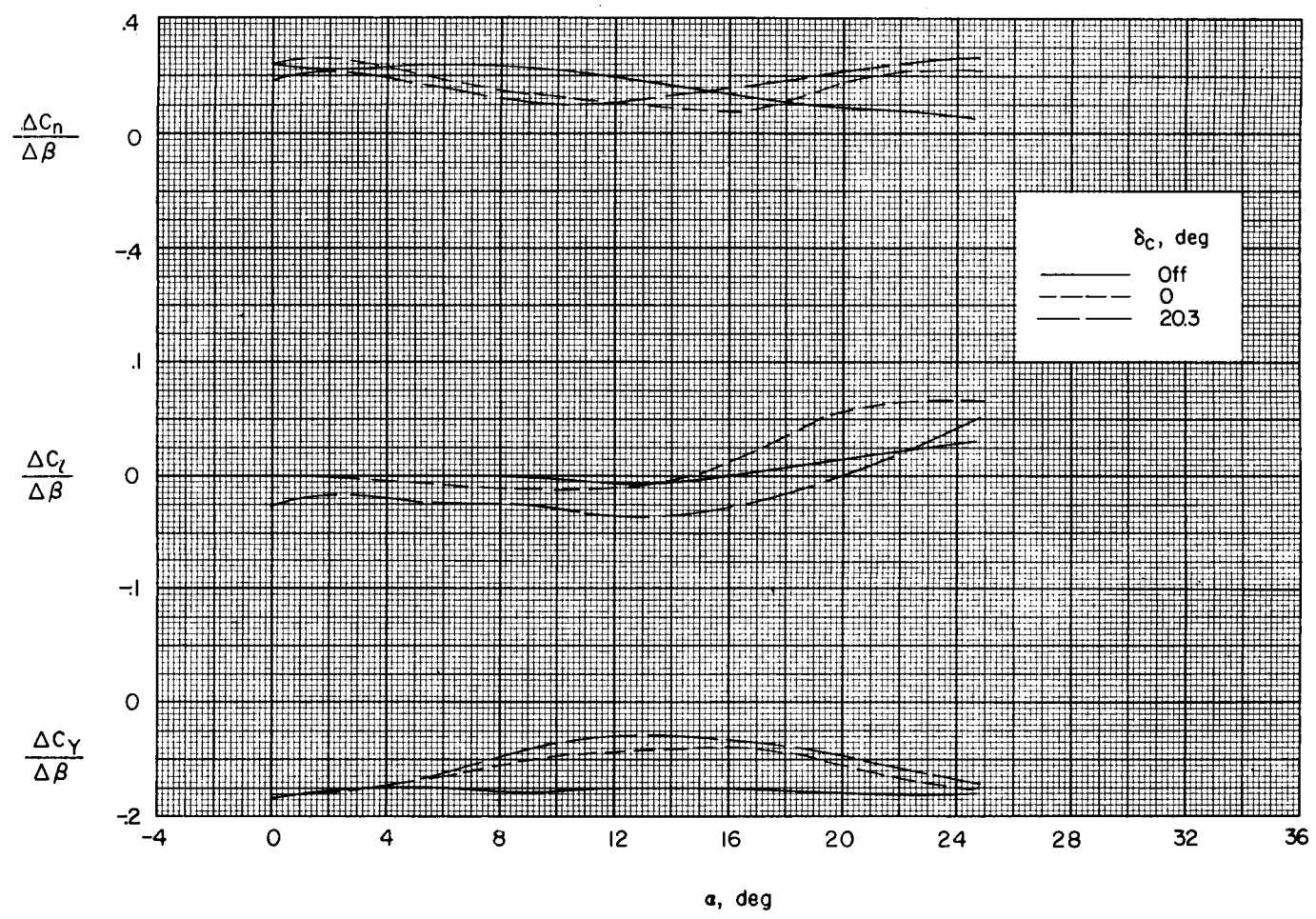
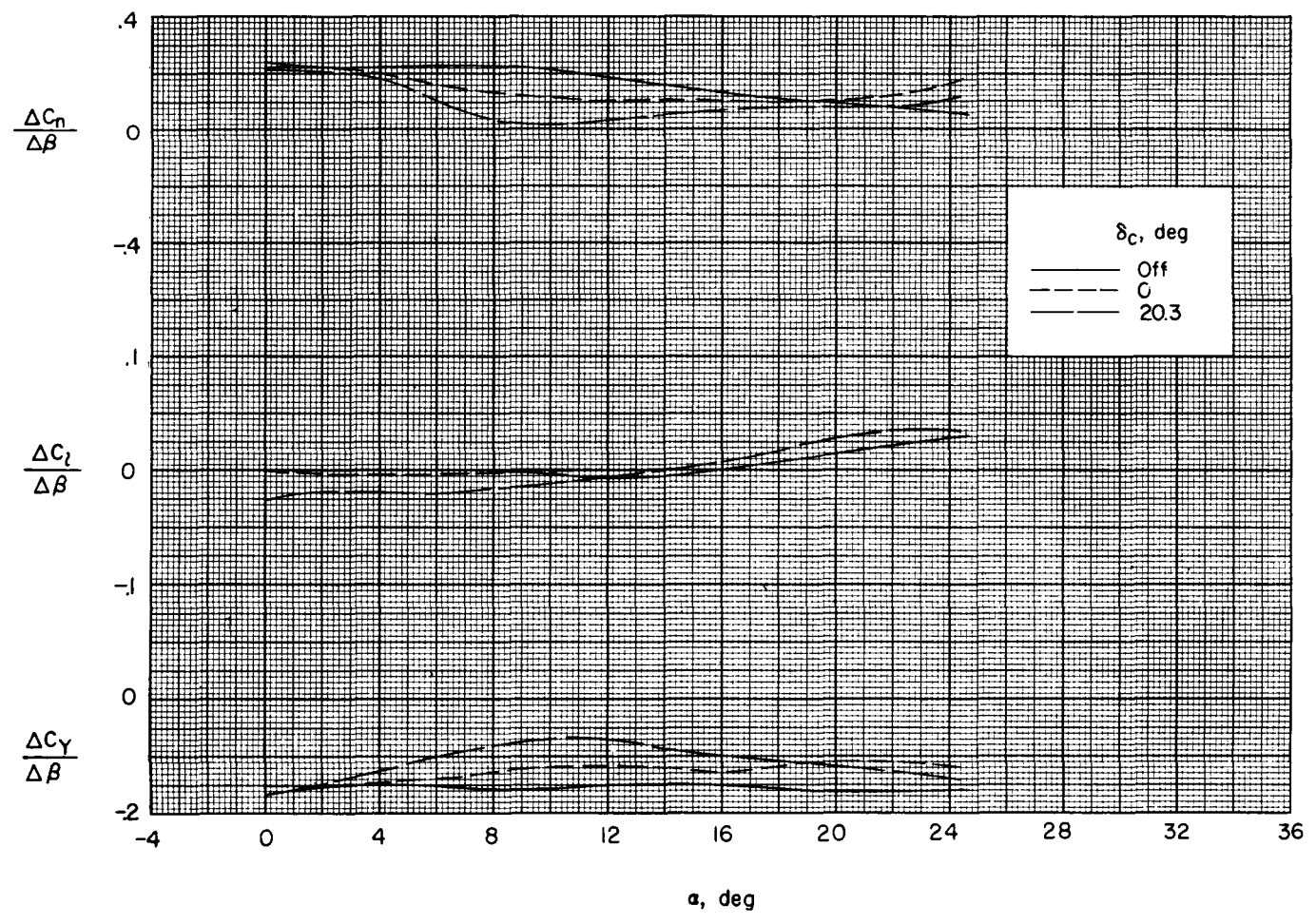
(a)  $C_1$ .

Figure 16.- Effect of canard deflection on the sideslip characteristics for the body with  $5^\circ$  fins configuration with various canards.



(b)  $C_2$ .

Figure 16.- Continued.



(c)  $C_3$ .

Figure 16.- Concluded.